Experimental and numerical study of the emission characteristics of a hot, dense plasma of multiply charged ions produced during liner acceleration in the ANGARA-5-1 device

G. S. Volkov, V. P. Gigiberiya, A. V. Kovalenko, S. A. Komarov, A. Yu. Sechin, V. P. Smirnov, A. N. Starostin, A. E. Stepanov, and V. Ya. Tsarfin

I. V. Kurchatov Institute of Atomic Energy, Moscow

(Submitted 11 July 1991)
Zh. Eksp. Teor. Fiz. **101**, 479–492 (February 1992)

Measurements of the line and continuum x-ray emission spectra of the plasmas of multiwire liners are reported. These measurements are interpreted on the basis of a detailed radiation-kinetics model of the kinetics of the various levels and of the radiation transport. The experiments were carried out at the ANGARA-5-1 device. The plasma was produced in the collapse of multiwire aluminum liners 3 cm long with a mass per unit length of 100–200 μg/cm. The current delivered to the load was 2.5–3 MA. According to the measurements, the total power was 1–1.5 TW. Of this, 0.3–0.4 TW was in the line emission of H- and He-like ions. Corresponding calculations show that the emission from the liner plasma can be described well by the model of a uniform plasma cylinder with a radius of 1 mm, a density of $2.5 \cdot 10^{-3}$ g/cm^3, and a temperature of 240 eV, which contracts at a velocity of $2.5 \cdot 10^7$ cm/s. If the motion of the plasma is ignored, one cannot reproduce the entire set of experimental data in the calculations.

An interesting application of generators of nanosecond-range electrical pulses is generating intense fluxes of soft x radiation through the electrodynamic acceleration and compression of cylindrical liners. This application has been developing rapidly over the past few years. The plasma formed as a result of the liner collapse has a temperature of 0.1–1 keV and a density on the order of 10^{-3} g/cm^3 (Ref. 1). It has a typical diameter of 1–3 mm and a typical length of 1–3 cm. This plasma emits well in the vacuum-*uv* and soft-x-ray regions. In this paper we report experimental results carried out with multiwire aluminum liners at the high-power ANGARA-5-1 pulse generator ($P \approx 10$ TW). We interpret these results on the basis of a detailed radiation-kinetics model.

1. EXPERIMENTAL RESULTS

We studied the plasma produced during the collapse of a multiwire ($N = 8$) aluminum liner between the cathode and anode of the output unit of the device. The initial diameter of the liner was 15–30 mm, its height was 30 mm, and its mass per unit length was 200–100 μg/cm. A current with an amplitude of 2.5–3 MA, with a rise time ≈ 80 ns, was passed through the liner. The initial diameter of the liner and its mass per unit length were chosen to match the generator with the load represented by the liner.[2] A smaller initial diameter corresponded to a higher mass per unit length.

The soft x radiation was detected in a direction perpendicular to the liner axis. The part of the spectrum between 10 eV and 5 keV was measured with vacuum x-ray diodes by the filter method. Specifically, we used photodiodes with aluminum photocathodes behind various filters: 40 μg/cm^2 of nitrocellulose lacquer, 420 μg/cm^2 of Mylar, 840 μg/cm^2 of Mylar, 420 μg/cm^2 of Mylar plus 270 μg/cm^2 of aluminum, and no filter at all. To keep the detectors in linear operation in the case without a filter and in the case with the nitrocellulose lacquer filter (40 μg/cm^2), we used "neutral" filters which attenuated the radiation flux by a factor of 16 without changing its spectrum. The "neutrality" of these filters was tested in a separate control experiment. Data on the quantum efficiency of the aluminum photocathode were taken from Ref. 3. The mass thickness of the filters was determined by weighing them. The mass attenuation coefficients of the various substances used as filters were taken from Ref. 4. Figure 1 shows transmission curves of the particular filters which we used.

In the spectral interval $0.8 \leqslant \hbar\omega \leqslant 6$ keV, the radiation was recorded on film by means of a crystal spectrograph. Specifically, we used a spectrograph with a convex mica crystal ($2d \approx 20$ Å). The crystal was bent to a radius of curvature of 25 mm. The spectrograph was positioned beside the liner axis, at a distance of 1.5 to 2 m from the source. Spectra were recorded with and without spatial resolution along the liner axis. In both cases, the dispersion direction of the crystal was perpendicular to the liner axis. In the spatially resolved case, an image along the height of the liner was formed on the film by means of a slit between the liner and the crystal, oriented parallel to the dispersion direction of the crystal. The spatial resolution along the height of the object was ≈ 1.5 mm in this case. The spectral resolution $\lambda/d\lambda$ in the first and second orders of reflection was determined by the transverse dimensions (the diameter) of the

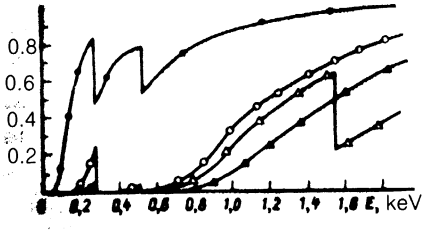

FIG. 1. Transmission curves of the filters used. ●—Nitrocellulose lacquer, 40 μg/cm^2; ○—Mylar, 420 μg/cm^2; ▲—Mylar 840 μg/cm^2; △—Mylar, 420 μg/cm^2 plus aluminum, 270 μg/cm^2.

 0038-5646/92/020253-08$05.00

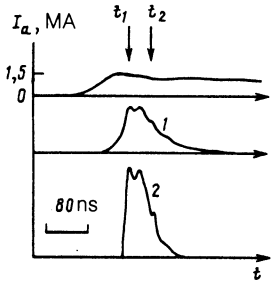

FIG. 2. Oscilloscope traces of the signals from the vacuum x-ray diodes behind various filters, synchronized with the accelerator current. The distance from the source to the detector is $L = 3$ m. *1*—Nitrocellulose lacquer filter, 40 μg/cm^2; *2*—Mylar filter, 3 μm, plus aluminum, 1 μm. (Aluminum liner, $m_l = 178$ μg/cm, diameter of 15 mm, $N = 8$.)

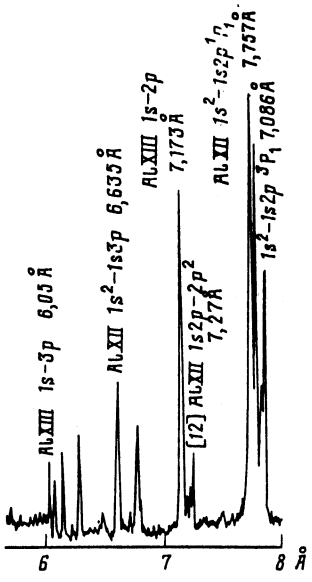

FIG. 3. Densitometer trace of the emission spectrum of an Al liner recorded by a crystal spectrograph with a curved mica crystal. In the first order of reflection, we have $E/\Delta E = 400$. (Liner with $m_l = 178$ μg/cm, with an initial liner radius $R_0 = 7.5$ mm.)

source along the dispersion direction. These resolution values were $R_1 = 400$ and $R_2 = 1100$ for $\lambda = 7.17$ Å. The resolution in the second order was comparable to the distance between the components of the L_α Al resonance doublet. The diameter of the plasma column was determined from the width of the line on the film in the first order of reflection. A time-integrated image of the plasma in soft x radiation was recorded with a pinhole camera.

The most interesting experiments were those with a mass per unit length $m_l \approx 200$ μg/cm and an initial diameter of 15 mm. In these experiments, the yield of radiation with $\hbar\omega \geqslant 1$ keV reached its highest levels. We restrict the discussion below to the results of the experiments with liners of these dimensions.

To measure the plasma spectrum we carried out a series of experiments in which the signals from five vacuum x-ray diodes, covered by various filters, were detected simultaneously. Figure 2 shows oscilloscope traces of the signals from these diodes, which detected radiation with $\hbar\omega \geqslant 80$ eV and $\geqslant 900$ eV. These signals were synchronized with the current through the liner. The signals reach their maximum at the same time, which corresponds to the maximum of the accelerator current. The ultrasoft radiation (line *1* in Fig. 2) begins about 50 ns after the current maximum and apparently corresponds to the emission of individual exploded wires. The duration of the emission at half-maximum is $\Delta t_{\text{tot}} = 70$ ns over the entire spectral range detected ($\hbar\omega \geqslant 10$ eV), while the duration for photons with $\hbar\omega \geqslant 900$ eV is $\Delta t_{\text{hard}} = 50$ ns.

It follows from the time evolution of the ratio of the signal amplitudes behind the various filters that the emission spectrum hardens after the emission begins and that the maximum hardness corresponds to the signal maximum. Analysis of these oscilloscope traces, with the help of the transmission curves of the filters which were used, leads to the conclusion that the emission spectrum of the liners has a fairly wide maximum at photon energies from 100 to 600 eV, while the spectral density of the emission at 600–1500 eV is low.

Figure 3 shows a densitometer trace of a part of the emission spectrum recorded by the crystal spectrograph. We see that the line emission of H-like and He-like ions of aluminum dominates in the spectrum at photon energies $\geqslant 600$ eV. The most intense lines are the L_α resonance doublet of the H-like aluminum ion and the resonance and intercombination lines of the He-like ion. Pinhole photographs recorded behind filters of beryllium (100 μm) and aluminum (6.5 μm) support the conclusion that most of the hard radiation is the line emission of H- and He-like ions of aluminum. The aluminum filter strongly absorbs the radiation at energies beyond the K absorption edge of aluminum, where we find the resonance lines of the H- and He-like ions of aluminum. On the pinhole photographs taken of the pinch behind these filters, through holes of identical area, the image behind the aluminum filter is much weaker than that behind a beryllium filter. The implication is that the radiation power is low in the energy interval 600–1500 eV, where the transmission of the aluminum filter is higher than that of the beryllium filter. It is thus natural to suggest that there is a second maximum in the emission spectrum, at photon energies corresponding to the resonance lines of H- and He-like ions of aluminum, with an amplitude several times smaller than that of the first. The radius of the region from which the hard radiation is emitted is ≈ 0.1 of the initial liner radius.

The problem of finding the spectral radiation density from known signals from detectors covered by various filters falls in the category of mathematically ill-posed problems. In the present study, we reconstructed the emission spectrum by making use of the iterative algorithm of Ref. 5. The choice of initial approximation is very important in problems of this type. From an analysis of the emission spectrum reported above and from an analysis of the signal amplitudes, we adopted the initial approximation illustrated in Fig. 4. Also shown in this figure are reconstructed spectra for the time $t_1 = 0$, which corresponds to the emission maximum, and for a time 40 ns after this maximum, $t_2 = 40$ ns (Fig. 2). An important point is that the solutions found here are stable with respect to pseudorandom perturbations of up to 20% in the signal levels. Such perturbations serve as a model of the errors in the experimental data on the signal amplitudes. Interestingly, the shape of the spectrum remains

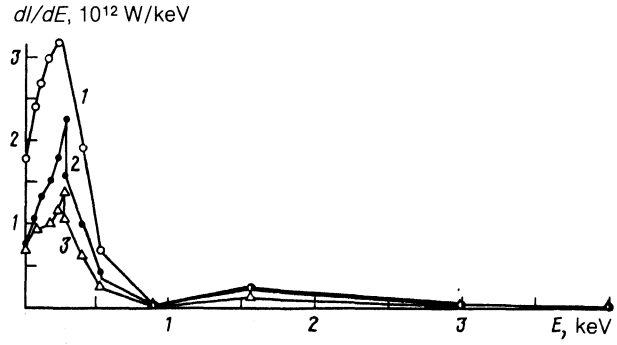

FIG. 4. Spectral emission density of an aluminum liner reconstructed by solving the inverse problem for various times. *1*—Initial approximation; *2*—spectrum at the time $t_1 = 0$ ns (Fig. 2); *3*—spectrum at $t_2 = 40$ ns (Fig. 2).

essentially constant as time elapses; the only change is a decrease in the signal intensity. The total radiated power is 1.2 TW; of this, 0.3 TW occurs in the region $\hbar\omega \geqslant 1$ keV. Taking the duration of the x-ray emission pulse, $\Delta t \approx 50$ ns, into account, we conclude that the total energy emitted by the liner at energies above 10 eV is 60 kJ. The maximum radiation power is less than the electrical power applied to the load by the generator. The apparent reason for this result is that the contraction of the liner is not compact. Laser shadow photographs and interferograms show that the wires evaporate completely even in the initial stage of liner acceleration, going into a plasma state. Estimates based on the laser shadow photographs show that, at the time at which the x-ray emission reaches its maximum outside the pinch, at least 30% of the initial mass of the wire liner is inside the region corresponding to the initial liner radius. Even at plasma velocities $\approx 3 \cdot 10^7$ cm/s, with an initial liner radius of 0.75 cm, emission can of course be maintained by the kinetic energy of the incident plasma for another ≈ 25 ns after the formation of the pinch.

As we have already pointed out, at $\hbar\omega \geqslant 600$ eV the line emission of H- and He-like ions of aluminum dominates (Fig. 3). In Fig. 3 we can clearly see satellites of the lines of the H-like aluminum ion. Along with the line emission, we find recombination jumps in the emission in the spectrum. These jumps correspond to recombination to the ground states of the H- and He-like ions, with respective series boundaries $\lambda = 5.39$ Å and $\lambda = 5.95$ Å. The energy in the line emission was determined from the signals from the vacuum x-ray diodes. It amounted to 10 kJ in the case of the liner 15 mm in diameter, with a mass per unit length $m_l = 178$ μg/cm.

2. NUMERICAL SIMULATION OF THE EMISSION PROPERTIES OF THE LINER PLASMA

Since fairly detailed information is available on the spectral characteristics of the emission from aluminum liners, we can use it for determination of the plasma pinch parameters in maximum compression phase, when a more or less homogeneous plasma cylinder with a radius $R_0 \approx 1$ mm. The duration of this stage (≈ 50 ns) is considerably longer than the time scales for the relaxation of the ion component and the populations of the excited levels. We thus use the quasisteady approximation. We can find the greatest amount of information on the spectral characteristics of the emission from the plasma of an aluminum liner by working from calculations based on a complete radiation-collisional model, allowing for radiation transport in the spectral lines and in the continuum. Previous work on numerical simulation of the emission spectra of Z-pinch plasmas is reviewed in Ref. 6. The numerical model which we used to interpret the experimental data on the spectral characteristics of the emission from the plasma of multiwire liners in the vacuum-uv and soft-x-ray regions incorporates the solution of the equations for the kinetics of the individual levels for the Li-, He-, and H-like ions of aluminum, along with the equation for radiation transport in the spectral lines and the continuum, in cylindrical geometry. The populations of the various states of the aluminum ions are found from the system of kinetic equations

$$\frac{d\mathbf{C}(r,t)}{dt} = \mathbf{K}\mathbf{C}(r,t). \tag{1}$$

The vector $\mathbf{C}(r,t)$ represents the set of relative populations of all the states taken into consideration, at the time t, at some spatial point r: $\mathbf{C}(r,t) = \{C_1(r,t),...,C_L(r,t)\}$; $C_l(r,t) = n_l(r,t)/n_{\text{tot}}(r,t)$, n_l is the population of level l ($l = 1,...,L$),and n_{tot} is the total density of all ions, i.e., $n_{\text{tot}} = \Sigma_l n_l$. The matrix $\mathbf{K}$ describes all possible elementary processes which lead to transitions between different states ($l < u$):

$$K_{lu}(r,t) = n_e\langle\sigma v\rangle_{ul}^{q} + A_{ul} + \alpha_{ul}^{rec} + B_{ul}\bar{J}_{ul}, \tag{2}$$

$$K_{ul}(r,t) = n_e\langle\sigma v\rangle_{lu}^{ex} + n_e\langle\sigma v\rangle_{lu}^{ion} + B_{lu}\bar{J}_{lu} + R_{lu}. \tag{3}$$

Here n_e is the electron density; $\langle\sigma v\rangle^{ex}$ and $\langle\sigma v\rangle^{q}$ are the rates at which a transition is excited and quenched by electrons; α^{rec} is the overall recombination rate, consisting of the rates of photorecombination, three-body recombination, and stimulated photorecombination; $\langle\sigma v\rangle^{ion}$ is the rate of electron-impact ionization of the lower level (l) with a transition to level u; A_{ul} are the Einstein coefficients for the probability for a spontaneous radiative transition; B_{ul} and B_{lu} are the Einstein coefficients for stimulated emission; and J_{ul} is given by

$$\bar{J}_{ul} = \frac{1}{4\pi}\int d\Omega \int d\omega\, I(r,\omega,\Omega)\,\Phi_{ul}\left(\omega - \omega_0\frac{\Omega\mathbf{v}(r)}{c}\right). \tag{4}$$

Here $I(r,\omega,\Omega)$ is the radiation intensity, which depends on the spatial point, the frequency, and the solid angle (Ω is a unit vector along the direction in which the photon is moving); ω_0 is the transition frequency; and Φ_{ul} is the spectral lineshape. We are using the approximation in which the energy is completely redistributed among the frequencies,[7] so we write $\Phi_{ul} = \Phi_{lu}$ and $\bar{J}_{ul} = \bar{J}_{lu}$. The photoionization rate is

$$R_{lu} = \int d\Omega \int_{I_l}^{\infty} d\omega\, \sigma_{lu}^{ph}(\omega) I(r,\omega,\Omega)/\omega, \tag{5}$$

where I_l is the ionization potential of level l, and $\sigma_{lu}^{ph}(\omega)$ is the photoionization cross section. It is assumed in (4) and (5) that the frequency ω is expressed in energy units. The radiation intensity is found from the equation

$$(1-\gamma^2)^{1/2}\left(\mu\frac{\partial I}{\partial r} + \frac{1-\mu^2}{r}\frac{\partial I}{\partial \mu}\right) = -kI + \varepsilon, \tag{6}$$

where μ and γ are the cosines of the angles specifying the direction in which the photon is moving in the case of cylindrical geometry (Ref. 8, for example); k is the overall absorption coefficient, representing the absorption in a spectral line (or in several lines, if they overlap) and in the continuum; and ε is the total emissivity, which is again a sum, of the emissivities in the spectral lines and in the continuum. The emission and the absorption in the continuum are consequences of bremsstrahlung, inverse bremsstrahlung recombination radiation, and the absorption of photons, in the course of photoionization. To solve Eqs. (1)–(6), which constitute a nonlinear system of equations, we use Newton's method, which results in a fairly rapid convergence of the iterative process over a broad range of plasma parameters. The model which we are using does not lean on the approximations used in Ref. 9, where radiation transport was taken into account only for the resonance lines, in the highly simplified model based on a two-level atom, and the ion composition was found in a non-self-consistent way in the coronal approximation.

In most cases, the calculations were limited to the levels of the H- and He-like ions with principal quantum numbers $n \leqslant 3$ and the Li-like ions with $n \leqslant 5$. The fine structure of the levels was taken into account in the model. The levels of other aluminum ions were ignored, since their populations were negligible under the conditions considered here. A total of 45 states were included in the calculations. The program allowed us to vary the number of states taken into consideration for each ion and also to incorporate ions with other charges. The energy levels and the radiation oscillator strengths were calculated from the programs of Refs. 10 and 11. Those of the H-like ions were instead taken from the tables of Refs. 12 and 13. The rates of transitions driven by electron impact were taken from Refs. 14–16 for the most part; where necessary, they were calculated by the Atom program.[17] The semiempirical Van Regemorter formula was used for transitions between highly excited states. The data of Ref. 14 and calculations by the Atom program were used for the rates of electron-impact ionization. Photoionization cross sections were calculated from the Kramers formula, with the hydrogen-like Gaunt factors from Ref. 13. A total of 112 radiative transitions leading to spectral lines and 215 transitions induced by electron impact were incorporated in the calculations.

In this formulation of the problem, the steady-state populations and the radiation field are determined by the spatial distributions of the temperature and the density (these distributions are assumed here to be flat) and by the spatial distribution of the plasma velocity (this velocity is assumed to be a linear function of the radius). It is very important to incorporate the motion, since the Doppler shift causes a large change in the optical thickness of the plasma in the resonance lines, a large change in the intensity ratios of certain lines utilized for plasma diagnostics, and a change in the spectral profile of the emission in the lines. The model thus has four parameters which determine the spectrum of the emitted radiation: the temperature T_0, the plasma density ρ_0, the cylinder radius R_0, and the velocity of the boundary, v_0. In the calculations we set R_0 equal to 1 mm.

Since the calculations carried out using the complete model were extremely expensive, we used a simplified zero-dimensional model to find rough estimates of the plasma parameters. In that model, it was assumed that the emission was a bulk emission and that the spatial distributions of all properties were flat. The effect of self-absorption of the radiation in the spectral lines was incorporated in this model through the introduction of a photon escape probability. This probability was assumed to be $\theta = \theta_D + \theta_S$, where θ_D is the probability for the escape of photons from the axis of the cylinder under the assumption of a Doppler lineshape, and θ_S is the probability for the escape of a photon in the Sobolev approximation.[18] The error of this approximation was checked by comparing the population at the cylinder axis with the results calculated in the approximation of a two-level atom. The parameters of the atom—the transition energy, the radiative-decay rate, and the rates of excitation and quenching—were chosen to correspond to the conditions for the formation of the resonance line of the He-like aluminum ion in the pinch plasma. The optical thickness at the center of the line was on the order of 10^3 in this case. It can be seen from Fig. 5 that the error associated with this approach of introducing a photon escape probability is small. Curve *2* in this figure was found from the model of a two-level atom under the assumption of a Voigt lineshape (the Voigt parameter was determined in the impact approximation). At velocities $v_0 > 5 \cdot 10^7$ cm/s, all three curves in Fig. 5 coincide, implying that the photon escape probability is determined by the motion of the medium and can be described well by the Sobolev approximation. At velocities $< 2 \cdot 10^7$ cm/s, the results calculated on the basis of a Doppler lineshape and the Sobolev theory are not sufficiently accurate; full-scale calculations become necessary in this case.

The model used for the calculations makes it possible to compare the following quantities with experimental data: (1) the total radiation power, $P_0 = 1.2$ TW; (2) the ratio of the energy radiated in the hard part of the spectrum to that radiated in the soft part, $\eta = 0.33$; (3) the ratio of the intensities of the resonance and intercombination lines of the He-like aluminum ion, $\alpha = 2.38$; (4) the ratio of the intensities

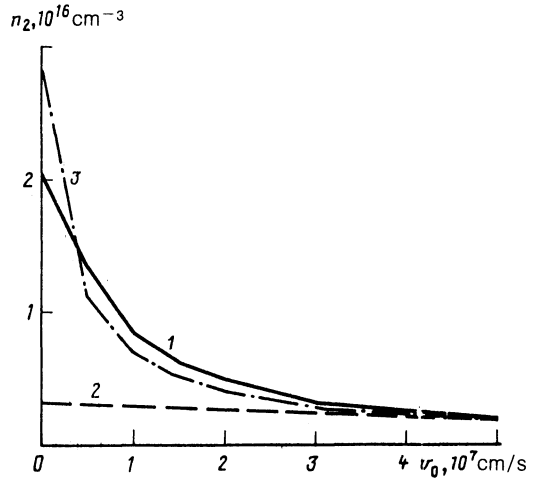

FIG. 5. Effect of the physical approximations and of the plasma velocity on the population of the upper level of a two-level atom ($n_1 + n_2 = 1.8 \cdot 10^{19}$ cm^{-3}, $n_e = 2 \cdot 10^{20}$ cm^{-3}, $T_0 = 250$ eV, $\hbar\omega = 1600$ eV). *1*—Equation (6), for radiation transport, with a Doppler lineshape; *2*—the same, but with a Voigt lineshape; *3*—zero-dimensional model with an escape probability (Doppler lineshape).

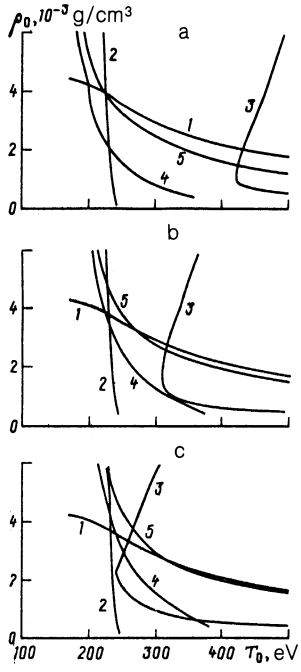

FIG. 6. Contour lines. *1*—The total emission power $P_0 = 1.2$ MW; *2*—relative amount of power radiated in the hard part of the spectrum $\eta = 0.33$; *3*—intensity ratio of the resonance line and of the intercombination line of AlXII $\alpha = 2.38$; *4*—intensity ratio of the AlXIII and AlXII resonance lines $\beta = 0.16$; *5*—ratio of the intensity of the $3p$–$1s$ line in AlXIII to the intensity of the resonance line of this ion $\gamma = 0.075$. a—$v_0 = 0$; b—$v_0 = -3\cdot10^7$ cm/s; c—$v_0 = -5\cdot10^7$ cm/s.

of the resonance lines of the H- and He-like ions, $\beta = 0.16$; and (5) the ratio of the intensity of the $3p$–$1s$ transition line in the H-like ion to that of the resonance line of this ion, $\gamma = 0.075$.

Using the zero-dimensional model, we plotted contour curves of these five quantities, corresponding to their experimental values, in the ρ_0, T_0 plane, for several values of v_0 (Fig. 6). If the experimental data are error-free, and if the model used for the calculations is appropriate for the physical situation, then all these contour curves should intersect at a common point, at a certain value of the velocity of the plasma boundary. As we see from Fig. 6, this is not quite what happens, but all the contour curves do converge fairly close together near the point $\rho_0 < 4\cdot10^{-3}$ g/cm^3, $T_0 = 250$ eV, $v_0 = 5\cdot10^7$ cm/s. We should point out that in the Sobolev approximation, and in the geometry which we have assumed, the photon escape probability does not depend on the direction of the velocity. In other words, an expansion of the plasma cannot be distinguished from a compression. This information can, on the other hand, be extracted from a comparison of the calculated plasma emission spectra and the experimental spectra in optically thick spectral lines. It can be seen from Fig. 6 that the intensity ratio of the resonance line and the intercombination line of the He-like aluminum ion is the quantity most sensitive to the velocity. For a plasma velocity $v_0 < 3\cdot10^7$ cm/s, we cannot reconcile all the experimental data with the calculations.

Let us take a more detailed look at the effect of the parameters of the pinch plasma on the ratio α of the intensities of the resonance line and the intercombination line of the He-like ion (AlXII). These lines are used widely to determine the densities of plasmas of multiply charged ions, because their intensity ratio in an optically thin plasma depends on the temperature and also—and fairly strongly—on the plasma density.[19] When the finite optical thickness of the plasma in the resonance lines is taken into account, the value of α begins to depend on the size of the plasma also. Moreover, at a given plasma size, the density dependence of α changes. This effect was noted in Ref. 20, where the intensity ratios of several spectral lines of H- and He-like aluminum ions were calculated as a function of the plasma density and temperature for homogeneous cylinders of three sizes (0, 50, and 100 μm) at rest. The effect of radiation reabsorption in the spectral lines was taken into account in that paper by introducing the photon escape probability.[21]

This effect can be studied qualitatively on the basis of a very simple three-level model (Fig. 7), which has only the $1s^2\,{}^1S_0$ ground state and two excited levels, $1s2p\,{}^1P_1$ and the $1s2p\,{}^3P_{0,1,2}$ combined level. The excitation rates of the $1s2s$ states are small in comparison with S_R and S_I (Fig. 7). The sublevels of a given multiplicity are mixed by electron impact at fairly high rates under the conditions considered here. Consequently, these states can be ignored in a first approximation. In this simplified level scheme, the intensity ratio of the lines under consideration can be written in a form which generalizes expressions of the type given in Ref. 19 to the case with radiation trapping (the notation is explained in the Fig. 7 caption):

$$\alpha = \frac{I_R(\mathrm{He})}{I_I(\mathrm{He})} = \frac{A_R\theta_R}{G\delta A_I\theta_I}\left(1 + \frac{S_R}{GS}\,\frac{GA_I\theta_I\delta + A_R\theta_R}{S_I\delta + S_R}\right), \qquad (7)$$

where $\delta = 1 + A_R\theta_R/GS$. The effect of radiation reabsorption is taken into account by multiplying the probability for a radiative transition by the probability that a photon will escape from the plasma volume under consideration.

We restrict the discussion to the case $\hbar\omega_{R,I}/T_0 \gg 1$. In an optically transparent plasma, at very high densities, at which the populations of all levels are determined by a Boltzmann distribution, we have $\alpha = A_R/GA_I \gg 1$, since the probability for a resonance transition is nearly three orders of magnitude higher than the probability for an intercombina-

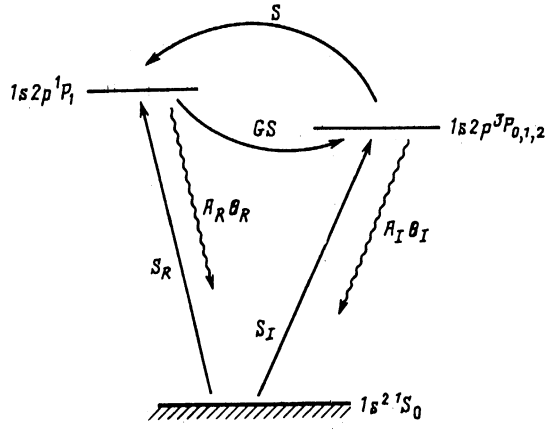

FIG. 7. Simplified level scheme used for the He-like ion for a qualitative study of the intensity ratio of the resonance and intercombination lines. S, S_R, S_I–Rates of electron-impact excitation of the levels; A_R, A_I–probabilities for radiative transitions; θ_R, θ_I–probabilities for photon escape in the resonance and intercombination lines; G–ratio of the statistical weights of the triplet and singlet levels.

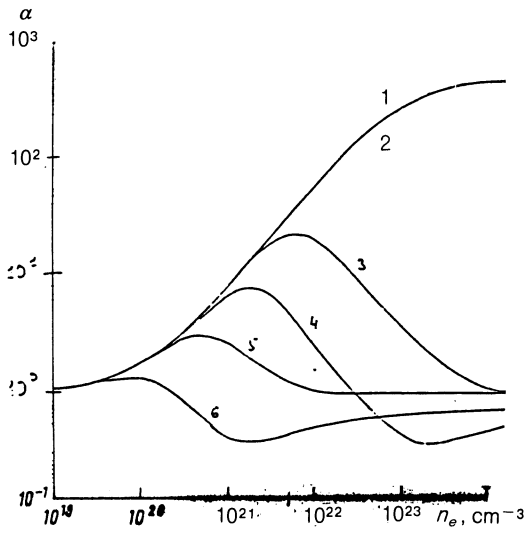

FIG. 8. The intensity ratio α of the AlXII resonance and intercombination lines versus the plasma density for various values of the pinch radius and the plasma velocity. *1*—$R_0 = 0$, $v_0 = 0$; *2*—$R_0 = 0$, $v_0 = -3\cdot10^7$ cm/s; *3*—$R_0 = 0.01$ cm, $v_0 = 0$; *4*—$R_0 = 0.01$ cm, $v_0 = -3\cdot10^7$ cm/s; *5*—$R_0 = 0.1$ cm, $v_0 = 0$; *6*—$R_0 = 0.1$ cm, $v_0 = -3\cdot10^7$ cm/s.

tion transition. For a Doppler lineshape, the probability for the escape of a photon from the axis of a uniform cylinder at rest is given by $\theta = 0.43/\tau(\ln\tau)^{1/2}$, where τ is the optical thickness at the center of the line. In the limit $\tau\to\infty$ we thus find $\alpha = (\ln\tau_I/\ln\tau_R)^{1/2} < 1$ (τ_R and τ_I are the optical thicknesses at the centers of the resonance line and the intercombination line).

The situation is even more complicated when the plasma motion is taken into account. If, as a result of a variation in plasma velocity, the frequency of a line shifts by an amount on the order of its width over distances shorter than the absorption length in the plasma at rest, the photon escape probability can be found from the Sobolev theory.[7,18] At large optical thickness we have $\theta_{ul} \sim 1/A_{ul}$, so the asymptotic value is $\alpha = 1$. In the intermediate region the photon escape probability may be much larger than the value found for a plasma at rest, so the value of α should also change markedly when the plasma motion is taken into account.

Figure 8 shows α as a function of the electron density according to (7) for a plasma temperature $T_0 = 250$ eV and an average ion charge $\langle Z\rangle = 11$, for various values of the cylinder radius R_0 and of the velocity v_0. It is easy to see that at cylinder radii 0.1–1 mm the quantity α cannot be used to determine the electron density in the usual way. Instead, it becomes necessary to carry out some fairly detailed kinetic calculations incorporating radiation transport. It can also be seen that at a pinch radius of 1 mm the value $\alpha = 2.38$, found experimentally, cannot be reproduced in the calculations, regardless of the plasma density, unless the motion of the plasma is taken into account.

A final refinement of the parameters of the pinch plasma was carried out on the basis of a comprehensive model incorporating the solution of both the kinetic equations and the radiation transport equations. The plasma parameter values which agree best with the set of experimental data are $\rho_0 = 2.3\cdot10^{-3}$ g/cm³, $T_0 = 240$ eV, and $v_0 = -2.5\cdot10^7$ cm/s (a negative value of v_0 corresponds to a plasma compression). The general shape of the plasma emission spectrum is shown in Fig. 9. Table I compares the calculated and experimental values of the quantities being modeled for several values of the velocity of the plasma boundary. The fraction of the emitted energy which is in spectral lines is 40%. The uncertainty in the plasma temperature found in this way is probably less than 20 eV (10%), and that in the plasma density and velocity is probably less than 30%.

Figure 10a shows the part of the spectrum near the resonance line and the intercombination line of the He-like aluminum ion according to the experimental data. The resonance line characteristically has a pronounced asymmetry, with two peaks. This shape is characteristic of a moving plasma. Figure 10, b–d, shows calculated emission profiles in the resonance line of the He-like aluminum ion for three velocities: $v_0 = 0$, $2.5\cdot10^7$, and $-2.5\cdot10^7$ cm/s. The calculations with the negative velocity agree with the experimental data and correspond to a contracting plasma.

To reduce the running time in the calculations, we assumed a Doppler lineshape. As can be seen from Fig. 5, at

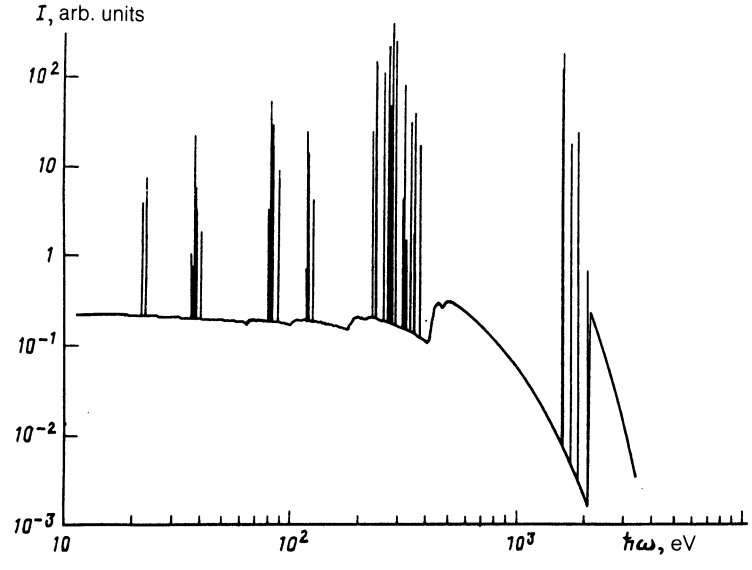

FIG. 9. Overall spectrum of the emission along the normal to the pinch axis.

TABLE I.

	$v_0=0$	$v_0=-1\cdot10^7$ cm/s	$v_0=-2.5\cdot10^7$ cm/s	$v_0=-4\cdot10^7$ cm/s	Experimental
P_0, TBT	1,09	1,22	1,3	1,41	1,2
η	0,49	0,50	0,52	0,60	0,33
$\frac{I_R(\mathrm{He})}{I_I(\mathrm{He})}$	0,841	1,76	2,35	3,31	2,38
$\frac{I_R(\mathrm{H})}{I_R(\mathrm{He})}$	0,58	0,22	0,15	0,1	0,16
$\frac{I_3(\mathrm{H})}{I_R(\mathrm{H})}$	0,093	0,058	0,052	0,045	0,075

I_R(He)—Intensity of the resonance line of the He-like ion, AlXII ($1s2p\ ^1P_1$–$1s^2\ ^1S_0$); I_I—intensity of the intercombination line of the He-like ion, AlXII ($1s2p\ ^3P_{0,1,2}$–$1s^2\ ^1S_0$); I_R(H)–intensity of the resonance line of the H-like ion, AlXIII($2p$–$1s$); $I_3(H)$—intensity of the $3p$–$1s$ line in AlXIII.

the velocity $v_0 \approx 3\cdot10^7$ cm/s a Voigt shape does not change the population greatly. Furthermore, for the plasma parameters which we are considering here, the collisional width of the resonance line of the He-like ion is smaller than its radiative width by nearly two orders of magnitude. Strictly speaking, the approximation of a complete frequency redistribution is not valid when this relation holds. However, calculations which we carried out with a partial frequency redistribution showed that the results found in the limit of a complete frequency redistribution, with a Doppler lineshape, are approximately the same as the results found in the approximation of a partial redistribution with respect to frequency.

CONCLUSION

This analysis has shown that the information found experimentally on the radiation by the plasmas of contracting multiwire liners is consistent. Within the framework of the model used here, this information corresponds to the emission by a homogeneous plasma cylinder of radius $R_0 = 1$ mm with a density $\rho_0 = 2.5\cdot10^{-3}$ g/cm^3, a temperature $T_0 = 240$ eV, and a velocity which varies linearly along the radius, from 0 to $-2.5\cdot10^7$ cm/s. The latter figure corresponds to contraction of the plasma. We do not believe that there are any experimental data presently available whose explanation would require incorporating variations in the plasma parameters along the pinch radius in the computation model, although the program which we used is easily capable of handling such complications. It was concluded in Ref. 22, on the basis of an analysis of the intensity ratios of spectral lines carried out in the coronal approximation, that the pinch plasma is inhomogeneous: The electron temperature and density are considerably higher near the axis than at the periphery. Our own calculations for a two-region structure of the pinch, as discussed in Ref. 22, show that the total radiation power is lower than that found experimentally by a factor of nearly 6. Moreover, the fraction of the radiation in the hard part of the spectrum is seriously overestimated.

We are deeply indebted to A. L. Godunov, Yu. K. Zemtsov, P. B. Ivanov, V. A. Makhrov, and V. A. Shchipakov.

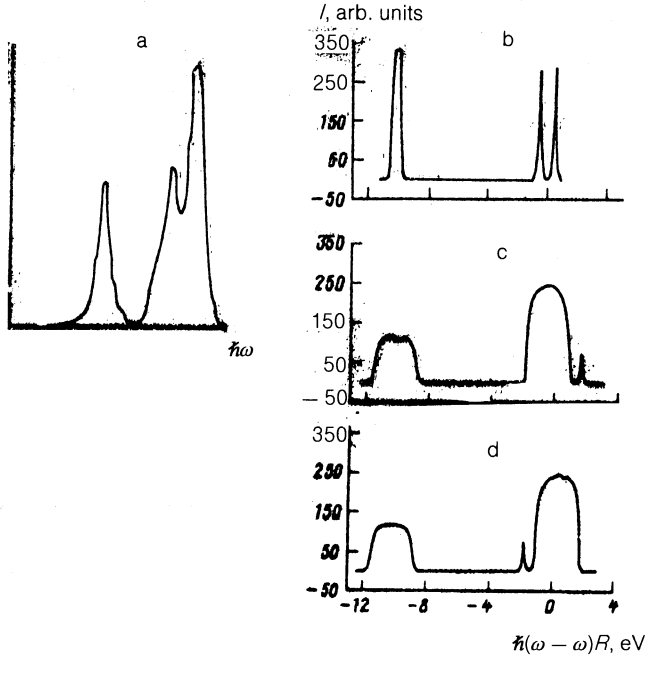

FIG. 10. Experimental (a) and calculated (b–d) profiles of the resonance and intercombination lines of AlXII. b—$v_0 = 0$; c—$v_0 = 2.5\cdot10^7$ cm/s; d—$v_0 = -2.5\cdot10^7$ cm/s.

[1] J. Pearlman *et al.*, in *Proceedings of the Fourth International Topical Conference on High-Power Electron and Ion Beam Research and Technology*, Palaiseau, France, 1981, p. 255.
[2] V. V. Zazhivikhin, I. K. Konkashbaev, L. B. Nikandrov, and V. P. Smirnov, Fiz. Plazmy **14**, 440 (1988) [Sov. J. Plasma Phys. **14**, 258 (1988)].
[3] R. H. Day and P. Lee, J. Appl. Phys. **52**, 6965 (1981).
[4] W. M. J. Veigele, At. Data Nucl. Data Tables **5**, 51 (1973).
[5] M. Z. Taraskin, E. A. Kramer-Ageev, and E. A. Tikhonov, *Radiation Dosimetry and Shielding*, Atomizdat, Moscow, 1970, No. 2, p. 125.
[6] N. K. Pereira and J. Davis, J. Appl. Phys. **64**, R1 (1988).
[7] D. Mihalas, *Stellar Atmospheres*, W. H. Freeman, San Francisco, 1978 (Russ. Transl. Mir, Moscow, 1982).
[8] B. N. Chetverushkin, *Mathematical Modeling of Problems in the Dynamics of Radiating Gases*, Nauka, Moscow, 1985.
[9] R. B. Baksht, I. M. Datsko, I. É. Gorel'chanik *et al.*, Fiz. Plazmy **15**, 1329 (1989) [Sov. J. Plasma Phys. **15**, 772 (1989)].
[10] K. G. Dyall, I. P. Grant, C. T. Johnson *et al.*, Comput. Phys. Commun. **55**, 425 (1989).
[11] R. D. Cowan, *The Theory of Atomic Structure and Spectra*, Los Angeles, California, 1981.
[12] G. W. Ericson, J. Phys. Chem. Ref. Data **6**, 831 (1977).
[13] W. J. Karzas and R. Latter, Astrophys. J. Suppl. **6**, 167 (1961).
[14] L. A. Vaĭnshteĭn, I. I. Sobel'man, and E. A. Yukov, *Excitation of Atoms*

and Broadening of Spectral Lines, Springer, New York (1951).
[15] S. J. Goett, R. E. H. Clark, and D. H. Sampson, At. Data Nucl. Data Tables **25**, 185 (1980).
[16] D. H. Sampson, S. J. Goett, and R. H. Clark, At. Data Nucl. Data Tables **29**, 467 (1983).
[17] D. A. Vaĭnshteĭn and V. P. Shevel'ko, *Structure and Characteristics of Ions in Hot Plasmas*, Nauka, Moscow, 1986.
[18] G. B. Rybicky and D. H. Hummer, Astrophys. J. **274**, 380 (1983).
[19] V. A. Boĭko, A. V. Vinogratsov, S. A. Pikuz *et al.*, in *X-Ray Spectroscopy of Laser Plasmas* (*Scientific and Technological Progress. Electronics Series*) (ed. N. G. Basov), Vol. 27.
[20] J. P. Apruzese, D. Duston, and J. Davis, J. Quant. Spectrosc. Radiat. Transf. **36**, 339 (1986).
[21] J. P. Apruzese, J. Quant. Spectrosc. Radiat. Transf. **25**, 419 (1981); **34**, 447 (1985).
[22] G. S. Volkov, S. A. Komarov, I. Yu. Faenov *et al.*, *Spectral Methods and Facilities for Measuring the Properties of Plasmas of Multiply Charged Ions*, VNIIFTRI, Moscow, 1988, p. 43.

Translated by D. Parsons